



Modelling cardiac fibrosis using three-dimensional cardiac microtissues derived from human embryonic stem cells

Mi-Ok Lee^{1*}, Kwang Bo Jung^{1,2}, Seong-Jae Jo^{1,2}, Sung-Ae Hyun³, Kyoung-Sik Moon³, Joung-Wook Seo³, Sang-Heon Kim^{4,5*} and Mi-Young Son^{1,2*} 

Abstract

Background: Cardiac fibrosis is the most common pathway of many cardiac diseases. To date, there has been no suitable in vitro cardiac fibrosis model that could sufficiently mimic the complex environment of the human heart. Here, a three-dimensional (3D) cardiac sphere platform of contractile cardiac microtissue, composed of human embryonic stem cell (hESC)-derived cardiomyocytes (CMs) and mesenchymal stem cells (MSCs), is presented to better recapitulate the human heart.

Results: We hypothesized that MSCs would develop an in vitro fibrotic reaction in response to treatment with transforming growth factor- β 1 (TGF- β 1), a primary inducer of cardiac fibrosis. The addition of MSCs improved sarcomeric organization, electrophysiological properties, and the expression of cardiac-specific genes, suggesting their physiological relevance in the generation of human cardiac microtissue model in vitro. MSCs could also generate fibroblasts within 3D cardiac microtissues and, subsequently, these fibroblasts were transdifferentiated into myofibroblasts by the exogenous addition of TGF- β 1. Cardiac microtissues displayed fibrotic features such as the deposition of collagen, the presence of numerous apoptotic CMs and the dissolution of mitochondrial networks. Furthermore, treatment with pro-fibrotic substances demonstrated that this model could reproduce key molecular and cellular fibrotic events.

Conclusions: This highlights the potential of our 3D cardiac microtissues as a valuable tool for manifesting and evaluating the pro-fibrotic effects of various agents, thereby representing an important step forward towards an in vitro system for the prediction of drug-induced cardiac fibrosis and the study of the pathological changes in human cardiac fibrosis.

Keywords: Cardiac fibrosis, Cardiac sphere, Cardiac microtissue, Cardiomyocyte, Mesenchymal stem cell

Background

Cardiac fibrosis is a common feature of most myocardial pathologies, including ischaemic cardiomyopathy, inherited cardiomyopathy mutations, metabolic syndrome, diabetes, and ageing [1, 2]. Increased mechanical stress or myocardial injury can trigger cardiac fibrosis, which might contribute to contractile and diastolic dysfunctions and

subsequent sudden death [3]. Cardiac fibrosis is characterized by the excess accumulation of extracellular matrix (ECM) components, such as collagen and fibronectin, with the consequent pathological remodelling of ECM, followed by transforming fibroblasts into myofibroblasts [4, 5]. These myofibroblasts have high fibrotic activity marked by the expression of α -smooth muscle actin (α -SMA), resulting in myocardial fibrosis and stiffening, which eventually impairs cardiac function [6, 7].

The exploration of the pathogenesis and therapy development for cardiac fibrosis is hampered by the lack of appropriate experimental models that fully recapitulate human cardiac fibrosis. An improvement of in vitro cell

* Correspondence: molee@kribb.re.kr; skimbrc@kist.re.kr; myson@kribb.re.kr

¹Stem Cell Convergence Research Center, Korea Research Institute of Bioscience and Biotechnology (KRIBB), Daejeon 341411, Republic of Korea
⁴Center for Biomaterials, Korea Institute of Science and Technology (KIST), Seoul 02792, Republic of Korea

Full list of author information is available at the end of the article



or tissue models may open up new possibilities for disease modelling, drug discovery, and regenerative medicine by providing fast and controllable platforms with high availability and relatively low cost compared to animal models. As yet, few in vitro models of cardiac fibrosis have been developed [8–12]. Most are composed of cardiac cells derived from neonatal mouse and rat hearts and thus have less relevance to human pathophysiology. In addition, most current models of cardiac tissue contain only cardiomyocytes (CMs) and lack other key cell types found in the human heart [13]. Therefore, there is a need for an in vitro human cardiac fibrosis model that possesses the physiologically relevant cell combination and can mimic the three-dimensional (3D) nature of native cardiac tissue.

Due to the limited amount of human primary CMs available, CMs derived from human pluripotent stem cells (hPSCs), including human embryonic stem cells (hESCs) and human induced pluripotent stem cells (hiPSCs), have emerged as the most appropriate cell source for modelling the human heart in vitro, with obvious advantages of multiple functionalities and increased throughput [14, 15]. Though hPSC-derived CMs or cardiac progenitor cells represent immature phenotypes in their morphological and other physiological and biochemical properties [16], there is a clear incentive to use hPSC-derived CMs as a foundation to generate 3D human cardiac tissue that can eventually be tailored to patient-specific models of normal and diseased cardiac tissues. However, to date, there are no suitable in vitro cardiac fibrosis model based on hPSC-derived 3D cardiac tissue to study the pathological changes in human cardiac fibrosis and to evaluate novel treatments.

In this study, we developed an in vitro model of cardiac fibrosis through hESC-derived 3D cardiac microtissues, composed of CMs and mesenchymal stem cells (MSCs) differentiated from the same hESC line. In the normal adult heart, CMs represent only 30% of the total cell number and the remaining 70% consists of various types of cells, among which cardiac mesenchymal cells are in the majority [17]. Cardiac mesenchymal cells can provide a major precursor population to generate fibroblasts, which mediate scar formation via fibroblast–myofibroblast transition during fibrosis [18–23]. Therefore, to engineer a physiologically relevant in vitro cardiac microtissues model, we used MSCs to provide fibroblasts, which can be differentiated towards myofibroblasts after stimulation with pro-fibrotic agents. The molecular and cellular properties of these 3D cardiac microtissues were characterized and the pro-fibrotic consequences were observed after induction with transforming growth factor- β 1 (TGF- β 1) or other pro-fibrotic mediators. We believe that our disease model using 3D cardiac microtissues may be a suitable in vitro model for

studying fibrotic changes in human heart tissue and can potentially contribute to the development of more physiologically relevant preclinical drug discovery platforms.

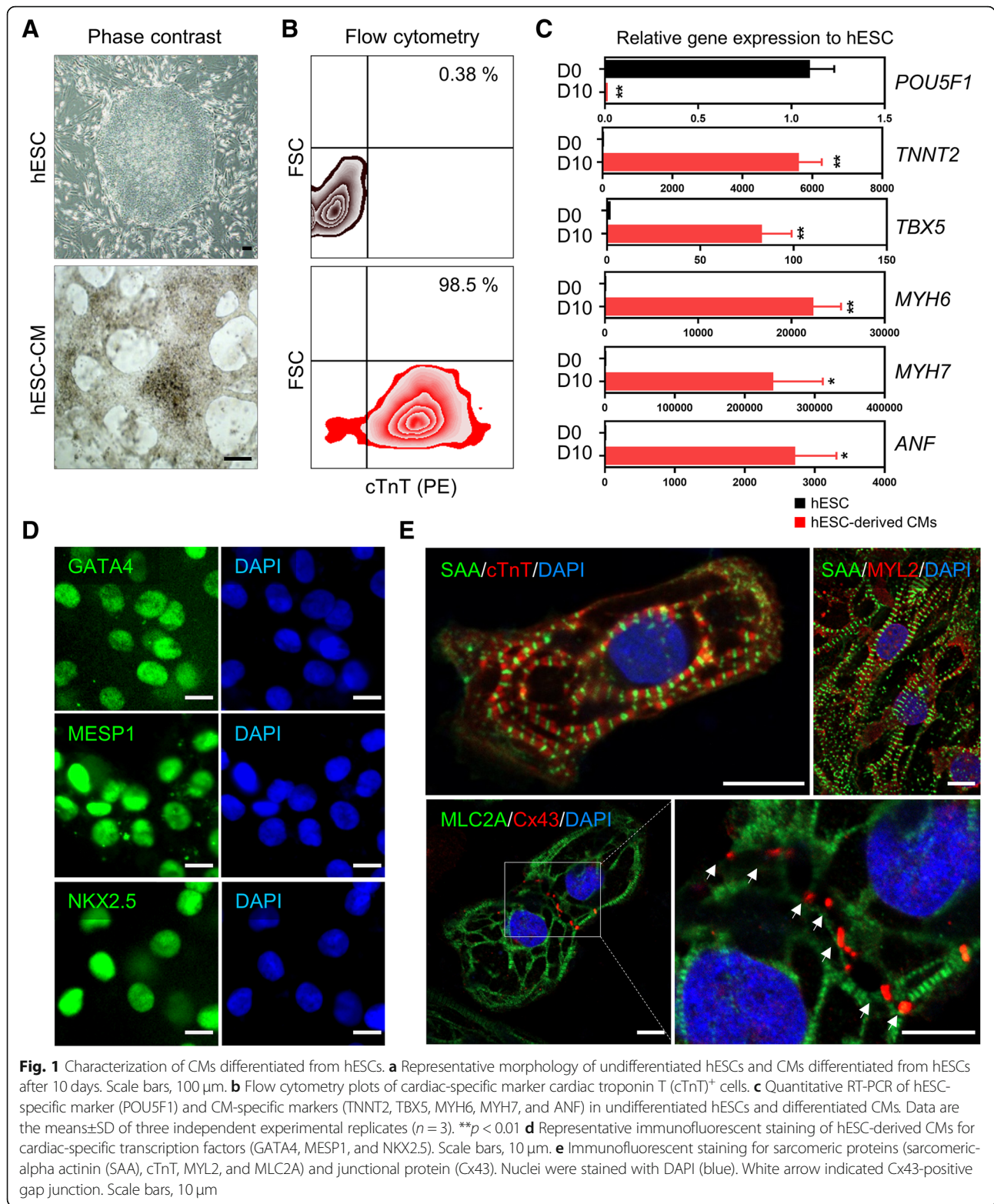
Results

Differentiation and characterization of CMs from hESCs

To obtain human CMs for the development of a human cardiac microtissue model, we differentiated hESCs, which can provide an unlimited source of starting cells for CM differentiation, into CMs by manipulating Wnt signalling as previously described [24]. At 8 days after the induction of differentiation, the synchronous and spontaneous beating areas were observed (Fig. 1a and Additional file 1: Movie 1). FACS analysis with CM-specific markers (cardiac muscle Troponin T (cTnT)) showed that hESCs were differentiated into CMs with high purity (> 98%) (Fig. 1b). The relative expression of *POU5F1*, a gene encoding an hESC-specific transcription factor, in differentiated CMs was markedly reduced compared with undifferentiated hESCs (Fig. 1c). By contrast, the expression of genes involved in the formation of sarcomere, the basic unit of myofibrils, including *TNNT2*, *MYH6*, and *MYH7*, and the peptide hormone gene (*ANF*) secreted in the cardiac muscle were significantly increased (Fig. 1c). We confirmed the expression of cardiac transcription factors (*GATA4*, *MESP1*, *NKX2.5*) in the nucleus (Fig. 1d), and further examined the formation of a myofibril structure responsible for contraction and relaxation of CMs and cardiac sarcomere by immunofluorescence for cTnT, *MYL2*, *MLC2A*, and sarcomeric alpha-actinin (*SAA*) (Fig. 1e). We showed the expression of the gap junctional protein Connexin 43 (*Cx43*), which plays an important role in the electrical coupling of myocardium [25], in the region of cell–cell interactions (Fig. 1e). Myofibrils stained with *MLC2A* were connected between the two cells via *Cx43* (Fig. 1e). These results showed that CMs differentiated from hESCs were interconnected via *Cx43*-mediated gap junctions, which have a similar structure to the *Cx43* gap junction plaque in the intercalated disc of cardiac muscle [26]. Overall, these data demonstrated that hESC differentiated into CMs with high purity and expressed cardiac function-related proteins, implying that hESC-derived CMs are appropriate cell sources for generation of an in vitro human cardiac tissue model.

Generation of 3D human cardiac microtissues

In this study, we attempted to simulate the pathological characteristics of cardiac fibrosis by introducing the 3D culture method. When 50,000 hESC-derived single CMs were seeded on round bottom 96-well ultra-low attachment plates, self-aggregation occurred slowly, resulting in uniform-sized cell spheroids (approximately 500 μ m



in diameter) (Additional file 2: Figure S1A). The created cardiac spheroids were beating at regular intervals and were maintained for more than 2 months (Additional file 3: Movie 2). TGF- β 1 signaling has been

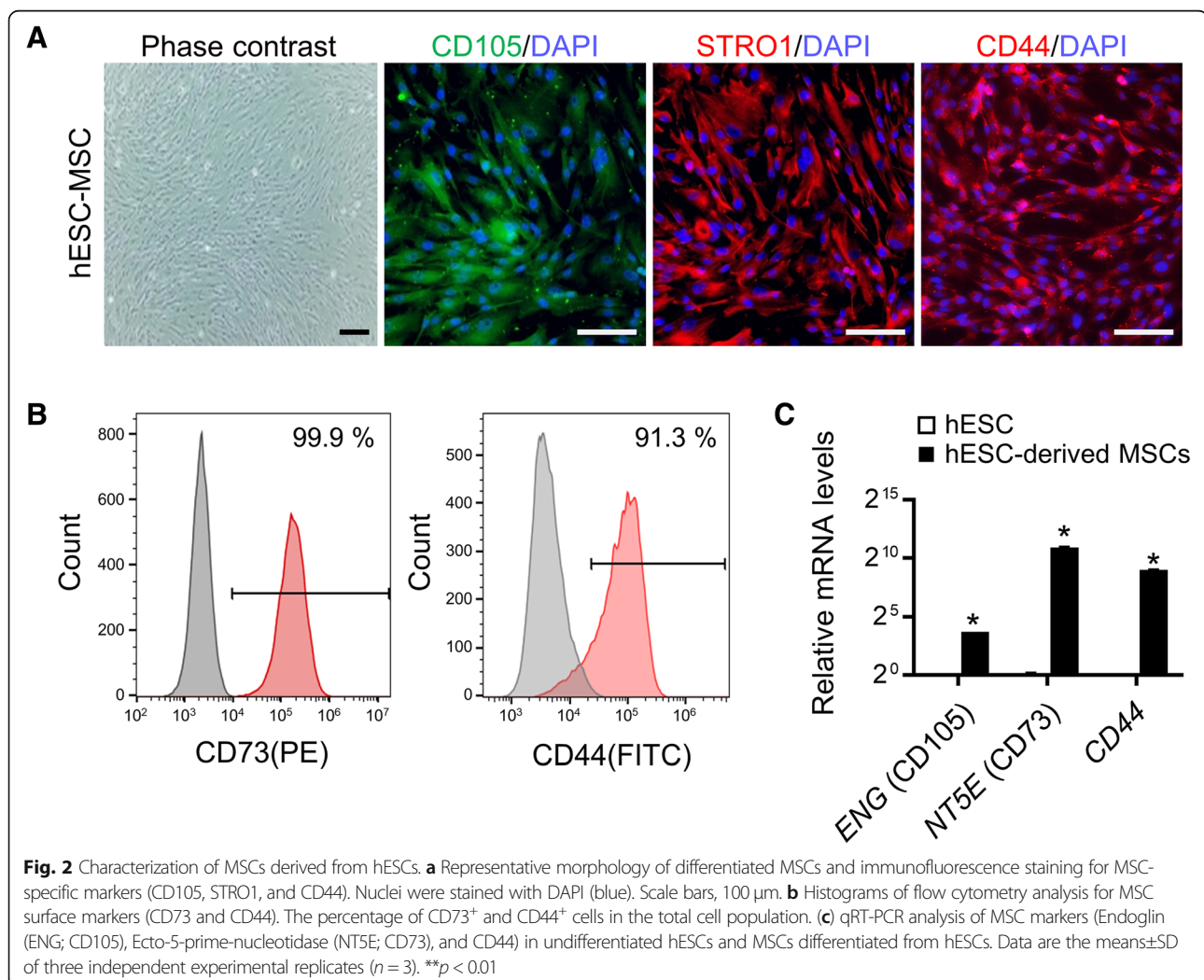
shown to play important roles in mediating fibrotic responses by regulating ECM remodelling and excessive collagen deposition, which eventually results in cardiac hypertrophy and fibrosis [27]. Therefore, we tested

whether cardiac fibrotic phenotypes can be reproduced by treating cardiac spheroids with TGF- β 1. However, TGF- β 1 treatment for 3 weeks did not show any marked effect on collagen deposition in the cardiac spheroids (Additional file 2: Figure S1B).

To establish a microtissue model that ultimately aimed to closely recapitulate human cardiac fibrosis, we used MSCs as a source of fibroblasts, which can be obtained by differentiation from the same hESCs used in differentiating into CMs. The expression of MSC surface markers such as CD105 and STRO-1 was confirmed by immunostaining and over 99% of the differentiated MSCs were in the CD73-positive populations (Fig. 2a, b). Most importantly, we found that most hESC-derived MSCs expressed CD44, a hyaluronic acid receptor and marker of cardiac MSCs [21], as evaluated by immunofluorescence and FACS analysis (Fig. 2a, b). qRT-PCR also confirmed that these differentiated MSCs expressed relevant markers, such as *ENG* (CD105), *NT5E* (CD73), and *CD44* (Fig. 2c). It has been previously reported that

endogenous CD44-positive MSCs contribute to the fibroblast population in myocardial infarction [18].

Therefore to develop a reliable 3D cardiac tissue model with increased physiological relevance, hESC-derived CMs were mixed with hESC-derived MSCs similar to those likely to be found in human cardiac tissue. In consideration of a report that cardiac fibroblasts account for 20% of total mass of the myocardium [28, 29] and the considerable variation of the ratio of cell numbers of fibroblasts in heart across studies [30], we tested various ratios of MSCs (5–20%), which are used as a source of fibroblasts in CM-MSC cardiac microtissues. Therefore, a single cell suspension of CMs was mixed at a 5–20% ratio of a single cell suspension of MSCs in round bottom 96-well ultra-low attachment plates to form cardiac microtissues called spheroids. Mixing with MSCs, known ECM-secreting cells, stimulated concentration-dependent formation of self-aggregates into cardiac microtissues (Fig. 3a). The average size of cardiac spheroids comprising



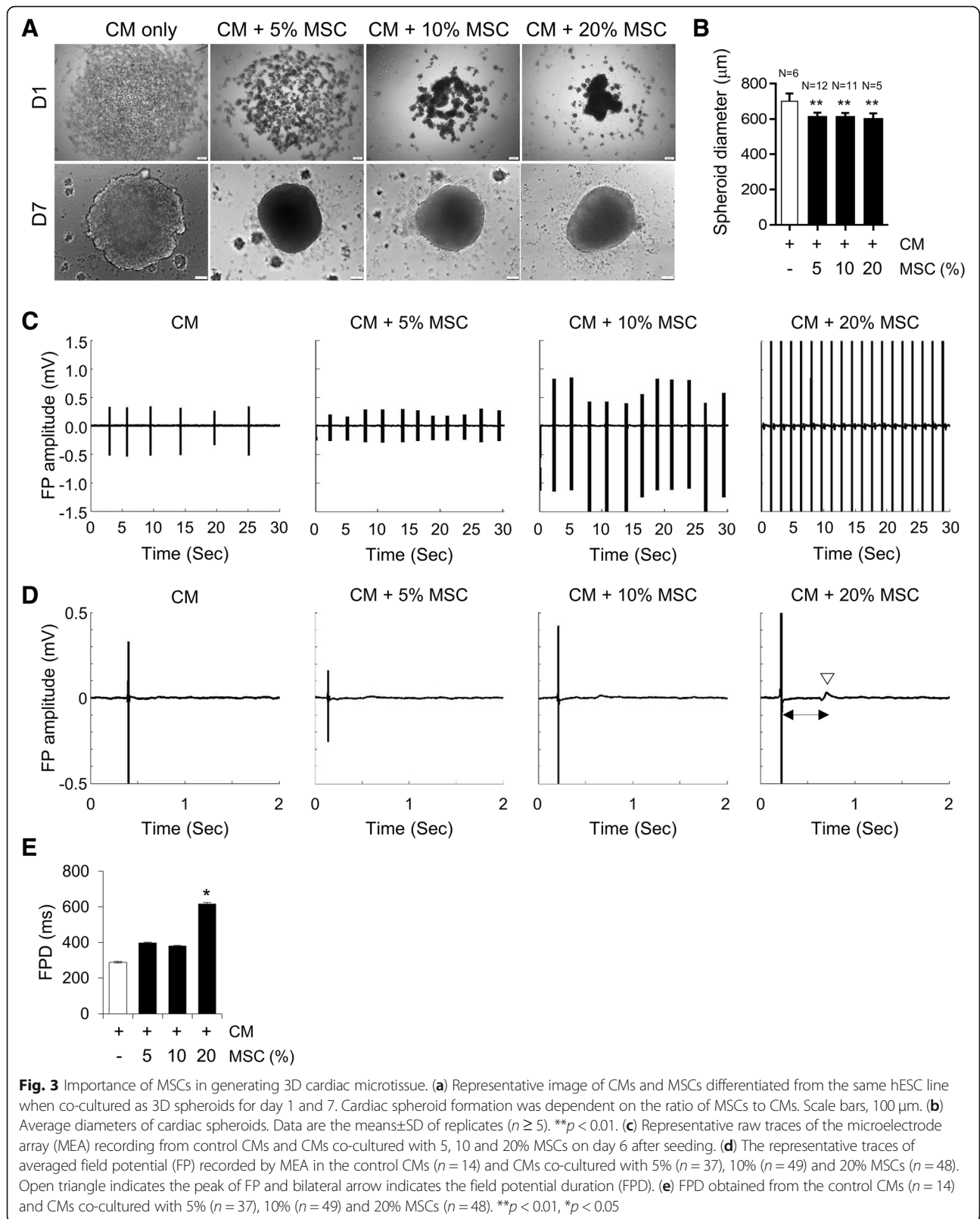


Fig. 3 Importance of MSCs in generating 3D cardiac microtissue. **(a)** Representative image of CMs and MSCs differentiated from the same hESC line when co-cultured as 3D spheroids for day 1 and 7. Cardiac spheroid formation was dependent on the ratio of MSCs to CMs. Scale bars, 100 μm . **(b)** Average diameters of cardiac spheroids. Data are the means \pm SD of replicates ($n \geq 5$). ****** $p < 0.01$. **(c)** Representative raw traces of the microelectrode array (MEA) recording from control CMs and CMs co-cultured with 5, 10 and 20% MSCs on day 6 after seeding. **(d)** The representative traces of averaged field potential (FP) recorded by MEA in the control CMs ($n = 14$) and CMs co-cultured with 5% ($n = 37$), 10% ($n = 49$) and 20% MSCs ($n = 48$). Open triangle indicates the peak of FP and bilateral arrow indicates the field potential duration (FPD). **(e)** FPD obtained from the control CMs ($n = 14$) and CMs co-cultured with 5% ($n = 37$), 10% ($n = 49$) and 20% MSCs ($n = 48$). ****** $p < 0.01$, ***** $p < 0.05$

hESC-derived CMs and 20% MSCs ($597.32 \mu\text{m} \pm 7.55$) was significantly smaller than that of CM only spheroids ($700.00 \mu\text{m} \pm 22.65$) (Fig. 3b). Cardiac spheroids comprising hESC-derived CMs and 20% MSCs also showed regular contractile activity (Additional file 4: Movie 3). To elucidate the electrophysiological features, we used an MEA system that enables simultaneous, accurate, and real-time recordings from multiple sites in the cell network [31]. MEA analyses revealed that CMs co-cultured with 20% MSCs showed a more regular spontaneous beating pattern with a beating frequency of approximately 49.15 ± 5.66 beats/min at 0 to 1 min than control CMs (17.81 ± 2.80 beats/min), CMs co-cultured with 5% (17.3 ± 0.63 beats/min) or 10% MSCs (26.1 ± 4.24 beats/min) (Fig. 3c). Furthermore, we observed a higher amplitude of field potential (FP) from CMs co-cultured with 20% MSCs compared with control CMs and CMs co-cultured with 5% or 10% MSCs (Fig. 3d). The field potential duration (FPD) of CMs co-cultured with 20% MSCs (616.82 ± 55.91 ms) was significantly increased compared to controls (288.66 ± 19.42 ms), CMs co-cultured with 5% (397.77 ± 20.81 ms) or 10% MSCs (380.23 ± 28.78 ms) (Fig. 3e), suggesting that the addition of 20% MSCs into 3D cardiac microtissues may promote functional improvement.

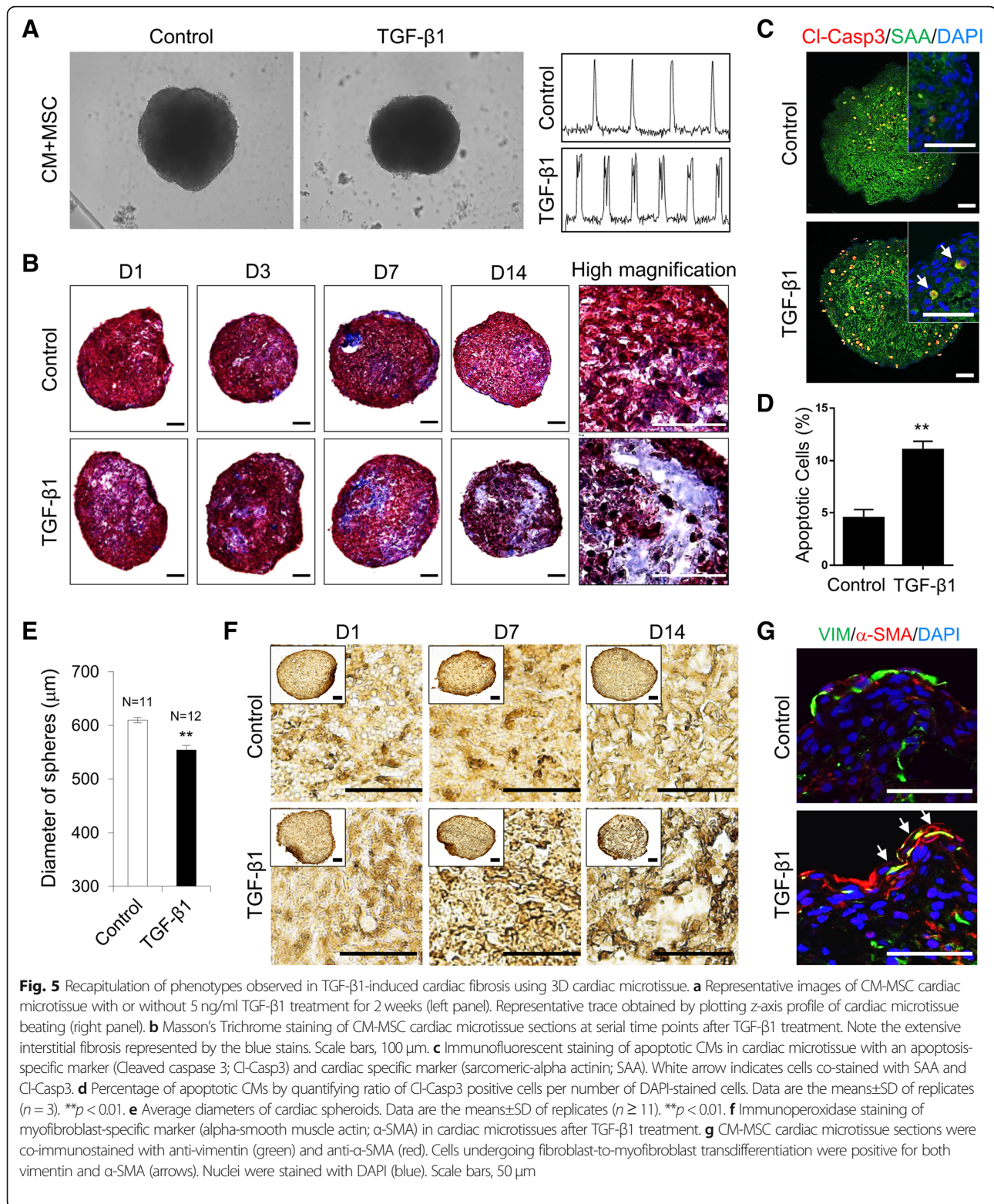
Characterization of 3D human cardiac microtissues

A comprehensive assessment of morphological integrity and cellular composition was conducted over cardiac microtissues by using immunofluorescence of key cell type-specific markers and cardiac gene expression analysis. Cardiac spheroids comprising CMs in combination with MSCs (CM-MSC cardiac microtissues) showed a compartmentalized organization in which SAA-positive CMs were concentrated in the center of the spheroid (Fig. 4a), while MSCs that were positive for vimentin, a mesenchymal and pan-fibroblastic marker, were at the periphery of the spheroid (Fig. 4a). Cells in the periphery of the spheroid also expressed the cardiac fibroblast-specific marker DDR2 (Fig. 4b, left panel), a collagen receptor expressed early in the adult heart and in development [32], which was not expressed in hESC-derived MSCs (Fig. 4b, right panel). Furthermore, vimentin and DDR2 double-positive cells emerged, suggesting a transdifferentiation of MSCs into fibroblasts within CM-MSC cardiac microtissues (Fig. 4b, arrows in left panel). Using PCA, we found that global transcriptomic data of CM-MSC cardiac microtissues clustered independently of control cardiac microtissues comprising only CMs, which were isolated from undifferentiated hESCs on principal component 1 (PC1, 51% variance), and became more similar to the transcriptome of the human heart (Fig. 4c). In addition, the transcriptome of the CM-MSC cardiac microtissues was distinct from that

of CMs and tended to be closer to the transcriptome of human heart on principal component 2 (PC2, variance 26%) (Fig. 4c). Further analysis of the transcriptomes revealed 746 differentially expressed genes (DEGs) in CM-MSC cardiac microtissues compared with control cardiac microtissues without MSCs. As expected, in the gene-set enrichment with increased genes in CM-MSC cardiac microtissues, a set of genes related to fibroblast function, such as cell signalling, com, and wound healing was predominantly identified (Fig. 4d). Consistently, pathways associated with cardiac muscle function, such as cardiac conduction and membrane depolarization during cardiac muscle cell action potential were also enriched in the DEG analysis (Fig. 4d). To confirm the regulation of genes related to cardiac muscle function by mesenchyme, the expression of the related genes was confirmed by qRT-PCR. In agreement with the microarray results, there was increased expression of genes related to cardiac function such as *SGCD*, which plays a role in dystrophin complex stabilization, *MYL1*, encoding the myosin light chain involved in cardiac conduction, and *SCN7A*, *SCN1B*, *KSNJ2*, and *KCNE4*, encoding voltage-gated ion channel related proteins (Fig. 4e). These results suggest that CM-MSC cardiac microtissues not only acquired fibroblastic functions by changing cellular composition but might also improve cardiac function through myocyte-mesenchyme interactions.

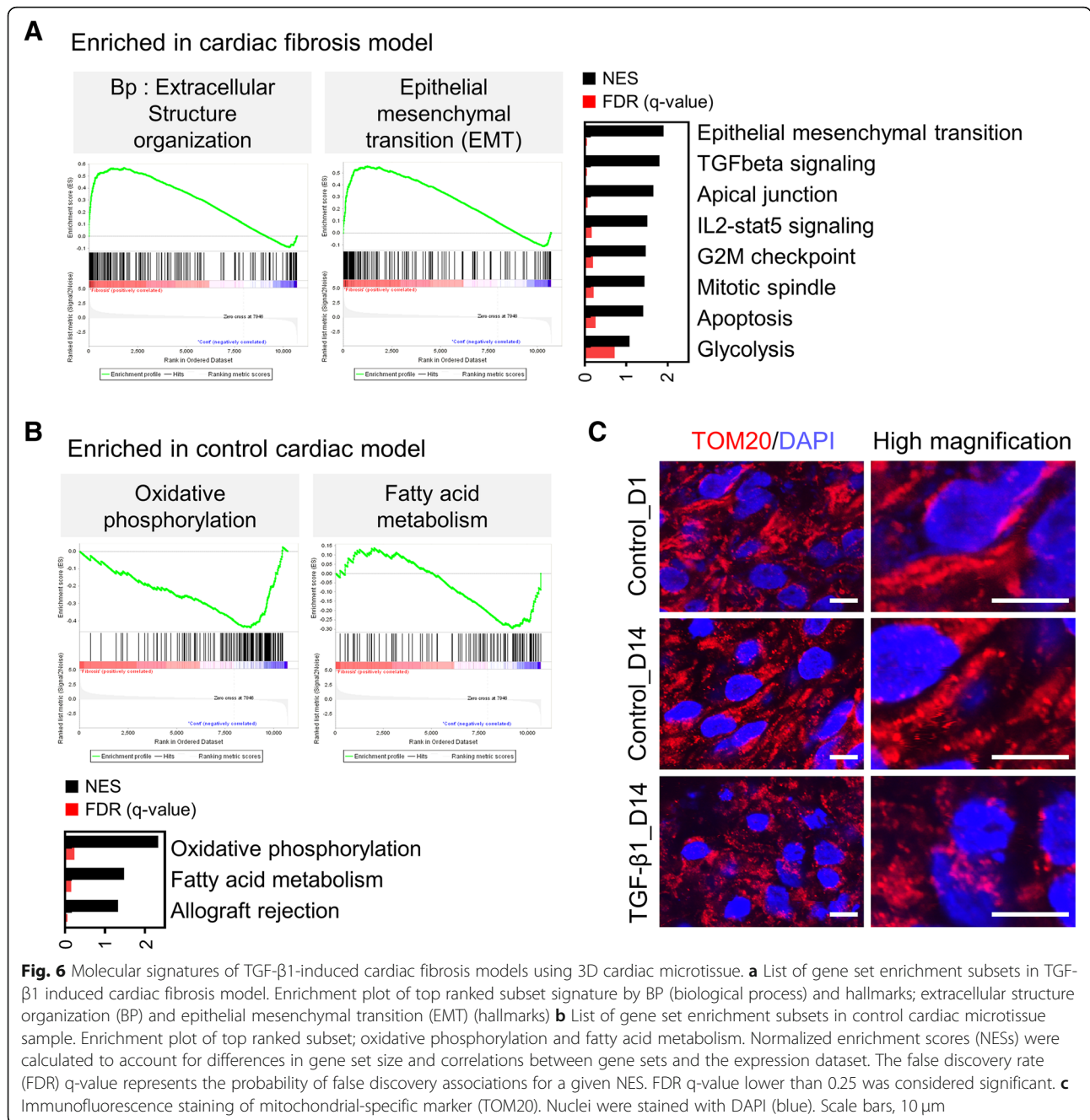
TGF- β 1-induced fibrosis in CM-MSC cardiac microtissues

To develop a fibrosis model using CM-MSC microtissues, they were treated with the pro-fibrotic growth factor TGF- β 1 for 2 weeks. Treatment of TGF- β 1 induced irregular beating patterns in cardiac microtissues (Fig. 5a and Additional file 5: Movie 4). To observe collagen deposition, Masson's Trichrome staining was performed in sections of TGF- β 1-treated CM-MSC microtissues in which a thicker collagen layer was detected after increasing the days of TGF- β 1 treatment as seen in fibrotic disease tissues (Fig. 5b). A highly consistent pattern of results was obtained by conducting repetitive experiments (Additional file 6: Figure S2). CMs of CM-MSC cardiac microtissues treated with TGF- β 1 exhibited significantly increased apoptosis as evidenced by increasing SAA/cleaved caspase-3 double-positive cells (Fig. 5c, d). The average sphere size was found to be approximately 10% smaller in TGF- β 1-treated CM-MSC microtissues ($554.17 \mu\text{m} \pm 14.87$) compared with the control ($610.36 \mu\text{m} \pm 8.06$) (Fig. 5e), which is the result of CM apoptosis. Furthermore, TGF- β 1 treatment also promoted the transdifferentiation of cardiac fibroblasts into myofibroblasts, a major cause of abnormal collagen secretion, as shown by the increased number of α -SMA-positive cells (Fig. 5f). In the TGF- β 1-treated group, α -SMA-positive cells increased over time (Fig. 5f). Most



enrichment analysis (GSEA) by biological process, hallmark and cellular localization was performed to identify functional biological pathways in TGF- β 1-induced fibrosis models (Fig. 6 and Additional file 7: Figure S3).

Consistent with the cellular phenotype shown in Fig. 5b, the extracellular structure organization was ranked as the upregulation pathway in the biological process analysis (Fig. 6a). Likewise, hallmark analysis showed an



increase in gene sets related to epithelial mesenchymal transition (EMT) and TGF-β signalling (Fig. 6a). In agreement with these data, GSEA by the cellular location demonstrated that proteinaceous extracellular matrix or the genes located on the basement membrane were enriched in the TGF-β1-induced fibrosis model (Additional file 7: Figure S3A). These analyses suggested that ECM deformation by TGF-β signalling was a major pathway in the fibrosis model. On the other hand, gene sets related to the respiratory chain or inner mitochondrial membrane proteins were enriched in the control

cardiac microtissue model (Additional file 7: Figure S3B). Consistent with these data, GSEA by the hallmark revealed that oxidative phosphorylation and fatty acid (FA) metabolism were decreased in the fibrosis model (Fig. 6b). These results raised the possibility that not only the accumulation of ECM as shown in Fig. 5b but also mitochondrial dysfunction may be induced in the TGF-β1-induced cardiac fibrosis model. To assess this possibility, we performed immunofluorescence of TOM20 to visualize the mitochondrial structure, which is closely related to mitochondrial function. Consistent

with previous studies [33, 34], the fragmented mitochondrial morphology was observed in cardiac microtissue treated with TGF- β 1, suggesting that mitochondrial dysfunction was induced in the cardiac fibrosis models (Fig. 6c). In addition, as FA metabolism is a predominant metabolic pathway in normal heart [35], changes in the expression of FA metabolism-related genes in fibrosis models may adversely affect the normal function of myocardial cells.

Drug-induced fibrosis in CM-MSC cardiac microtissues

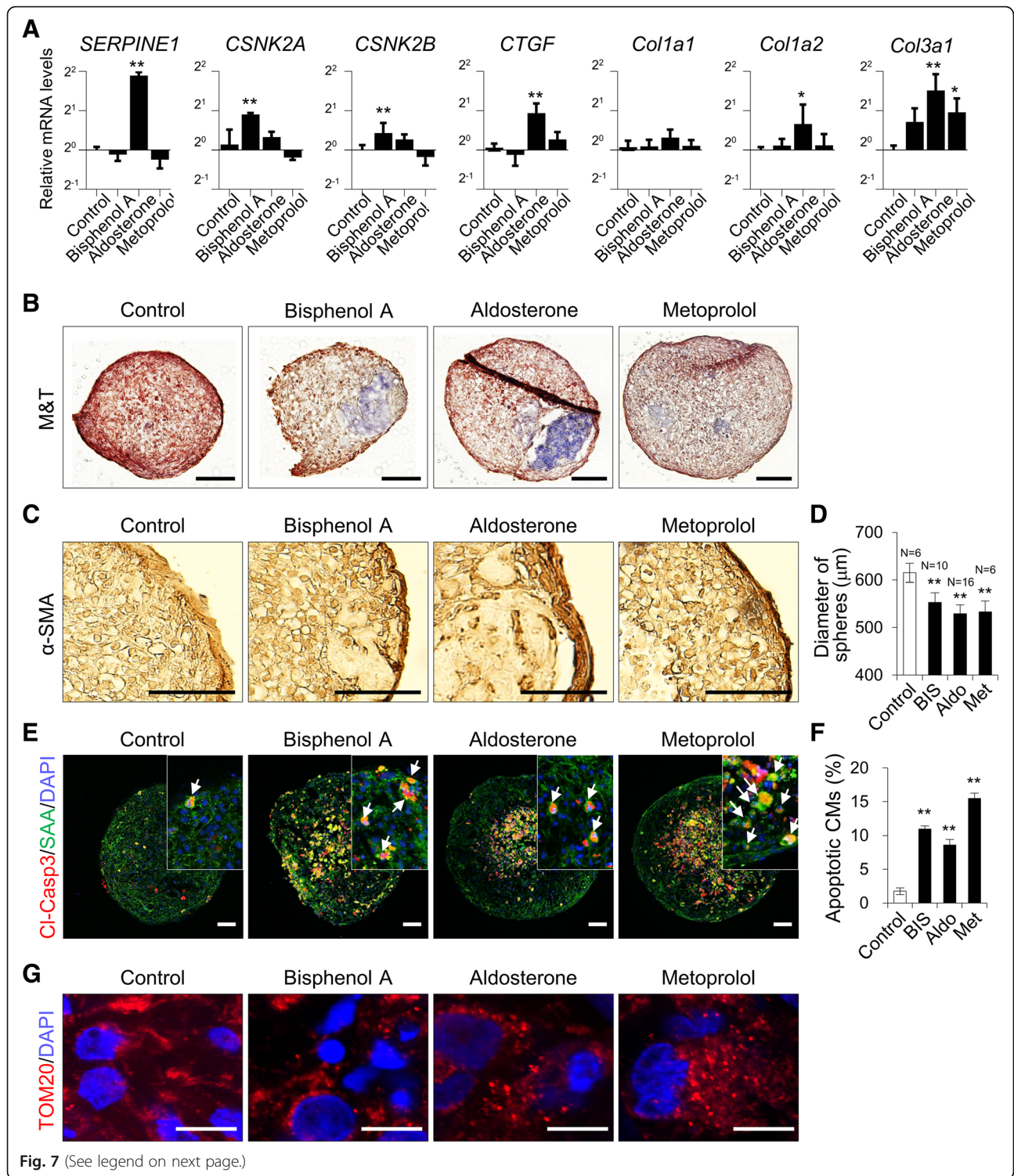
To further explore the applicability of CM-MSC cardiac microtissues to drug-induced cardiac fibrosis models, we examined reference pro-fibrotic mediators, including bisphenol A, aldosterone and metoprolol, which are known to induce cardiac fibrosis in vivo [36–38]. To explore drug responsiveness in the CM-MSC cardiac microtissue model, tissues were treated with each pro-fibrotic mediator at a concentration of 10 μ M for 2 weeks. qRT-PCR showed an increase in TGF- β 1-responsive genes, including *SERPINE1*, *CSNK2A*, *CSNK2B*, and *CTGF*, and collagen genes, including *COL1A1*, *COL1A2*, and *COL3A1*, although variations of responsiveness to each drug were observed (Fig. 7a). An increase in collagen deposition was seen in each compound-treated group compared with control CM-MSC cardiac microtissues (Fig. 7b). Hence, the contribution of pro-fibrotic mediators in transdifferentiation into myofibroblasts was examined in CM-MSC cardiac microtissues, as shown by immunohistochemistry with anti- α -SMA antibody (Fig. 7c). Among the three reference compounds, aldosterone was found to be the most effective for inducing fibrosis in our CM-MSC cardiac microtissues. The size of the spheres was significantly reduced after treatment with each compound (Fig. 7d). CMs of CM-MSC cardiac microtissues treated with reference compounds also exhibited significantly increased apoptosis as evidenced by increasing SAA/cleaved caspase-3 double positive cells (Fig. 7e, f). Moreover, mitochondrial phenotypes were confirmed in the drug-treated cardiac microtissues through TOM20 immunohistochemistry, indicating that mitochondrial fragmentation was increased by treatment with each drug (Fig. 7g). We examined whether treatment with pro-fibrotic drugs could directly influence CMs and the mitochondrial structure. There was no apparent apoptotic response or mitochondrial fragmentation in CMs (Additional file 8: Figure S4). Overall, 3D CM-MSC cardiac microtissues were able to recapitulate the pathological phenotypes of cardiac fibrosis, with differences in fibrotic responses depending on the drug. Therefore, the fibrosis model using CM-MSC cardiac microtissues will be an applicable model system for investigating mechanistic insights into fibrotic diseases

and in vitro screening of compounds for drug-induced cardiac fibrosis.

Discussion

The goal of engineering a 3D cardiac tissue model is to provide new opportunities for in vitro cardiac modelling with physiologically relevant cell types and microenvironment. The human 3D cardiac microtissue described in this study is expected to improve our knowledge about clinically relevant information regarding cardiac fibrosis and disclose advanced features of cardiac fibrosis. It is now widely believed that cultures of single cell types are very simplistic models, because they do not mimic the complexity and heterogeneity of human tissues. The normal heart is composed of several different cell types, such as CMs, endothelial cells, smooth muscle cells and fibroblasts, which play a role in the development of the heart and its normal functions [39]. Even within the in vitro environment, non-CMs influence the improvement of CM phenotypes and tissue architecture only in 3D cultures [40, 41]. These results are consistent with observations that most cell types do not exhibit the full spectrum of tissue-specific functionality in 2D cultures, since they do not maintain their phenotypes and patterns of gene expression precisely in the different environments compared with native tissue [42]. Therefore, to mimic the native cardiac tissue, our in vitro 3D co-culture strategy that includes relevant cell types appears most appropriate.

In this study, we have established for the first time a human 3D cardiac microtissue containing hESC-derived CMs in combination with hESC-derived MSCs. During heart development, fibroblasts, which are important cells that produce fibrotic ECM proteins [43], arise from multipotent progenitor cells, especially MSCs [19–21, 23, 44]. The cellular origins of cardiac fibroblasts are varied, including epithelial-mesenchymal transition (EMT) of epicardium cells, endothelial-mesenchymal transition (endo-MT) of epithelial cells, and MSCs [45]. Fibroblasts are connective tissue cells of mesenchymal origin that synthesize and secrete the main components of ECM, such as interstitial collagen and fibronectin [46, 47]. Fibroblasts also play an important role in fibrotic tissue formation by conversion into myofibroblasts under pathological conditions [48]. However, there is currently no standardized protocol for the reliable differentiation of hPSCs into cardiac fibroblasts, whereas, the differentiation methods of hPSCs into MSCs are well established [49, 50]. It has been also reported that MSCs can transdifferentiate into fibroblasts in vitro and in vivo [51]. Cardiac MSCs play an important role in preserving normal cardiac functions, as well as in cardiac remodelling at various pathological stages, by responding early to myocardial infarction [52]. Therefore we developed 3D



(See figure on previous page.)

Fig. 7 3D cardiac microtissue for in vitro assessment of drug-induced cardiac fibrosis. **a** qRT-PCR analysis for mRNA expression for fibrosis-related collagen genes (*Col1a1*, *Col1a2*, and *Col3a1*) and TGF- β responsive genes (*SERPINE1*, *CSNK2A*, *CSNK2*, and *CTGF*) in CM-MSC cardiac microtissues independently treated with 10 μ M concentration of each pro-fibrotic drug for 14 days. Data are the means \pm SD of three independent experimental replicates ($n = 3$). $**p < 0.01$, $*p < 0.05$. **b** Masson's Trichrome staining to detect collagen deposition in CM-MSC cardiac microtissues following treatment with pro-fibrotic drugs for 14 days. Scale bars, 100 μ m. **c** Immunoperoxidase staining of myofibroblast-specific marker (alpha-smooth muscle actin; α -SMA) in cardiac microtissues after treatment of pro-fibrotic drugs. Scale bars, 50 μ m. **d** Average diameters of cardiac spheroids. Data are the means \pm SD of replicates ($n \geq 6$). $**p < 0.01$. **e** Immunofluorescent staining of apoptotic CMs in cardiac microtissue with an apoptosis-specific marker (Cleaved caspase 3; Cl-Casp3) and cardiac-specific marker (sarcomeric-alpha actinin; SAA). White arrow indicates cells co-stained with SAA and Cl-Casp3. Scale bars, 50 μ m. **f** Percentage of apoptotic CMs by quantifying ratio of Cl-Casp3 positive cells per number of DAPI-stained cells. Data are the means \pm SD of replicates ($n = 4$). $**p < 0.01$. **g** Immunofluorescence staining of mitochondrial-specific marker (TOM20). Nuclei were stained with DAPI (blue). Scale bars, 10 μ m

cardiac microtissues consisting of CMs in combination with MSCs as a source of fibroblasts for developing the in vitro cardiac fibrosis model. The generation of cardiac spheroids with hESC-derived CMs and MSCs has an advantage in terms of the spheroid formation time. As shown in Fig. 3a, aggregates started to form only 1 day after seeding CMs mixed with 20% MSCs, and compact and circular spheroids were successfully generated, whereas loose aggregates with poor cell-cell contacts were formed when CM was cultured only in 3D. Consistent with our findings, Ong et al. have shown that multicellular cardiac spheres are generated from hiPSC-CMs only when they are mixed with human adult ventricular cardiac fibroblasts and human umbilical vein endothelial cells [53]. Furthermore, increased expression of sets of genes associated with ECM organization and cell adhesion (Fig. 4d), which are known to be essential for sphere formation [54], in CM-MSC cardiac spherical microtissues allows more rapid sphere formation in comparison to CM spheroids.

DDR2 is known to be selectively expressed in cardiac fibroblasts [45, 46, 55], although it appears to be also expressed in pericytes/vascular smooth muscle cells [56]. As shown in Fig. 4b, all of vimentin-positive MSCs were not co-expressed with DDR2, whereas some cells within CM-MSC cardiac spheroids were double-positive for vimentin and DDR2, suggesting a transdifferentiation of MSCs into fibroblasts within CM-MSC cardiac spheroids. Our findings are supported by a report that CD44-positive MSCs served as a major precursor pool for fibroblasts that mediate scar formation and wound healing after myocardial infarction [18]. In addition, bone marrow-derived MSCs [57, 58] and perivascular-resident MSCs [59, 60], as well as cardiac fibroblasts, which are known to be direct sources of myofibroblasts and MSCs, also exhibit myofibroblastic phenotypes in vitro in response to TGF β treatment [61].

As in previous cardiac fibrosis models, mouse and rat neonatal CMs are commonly used for developing engineered cardiac tissue because terminally differentiated adult CMs cannot proliferate sufficiently in vitro [8, 10, 12]. In this study, CMs derived from hESCs were well characterized by the expression of cardiac

function-related proteins (Fig. 1a-e). Particularly, CMs were connected to each other by the intercalated disc structure by using immunofluorescence staining of Cx43, the most abundant cardiac gap junction protein (Fig. 1e). Cx43 expression was observed as dots in the intercellular connected regions, in which the ends of myofibrils were connected, consistent with a previous study [62]. hPSC-derived CMs have been widely used to perform drug and toxicity testing in vitro [63, 64]. Furthermore, CMs differentiated from hiPSCs generated from patients with genetic cardiac diseases also allow for the generation of CMs carrying the genetic background of a given patient, creating highly tailored models for cardiac diseases in vitro [65]. Recently, a cardiac model of multicellular systems with several cell types, including CMs, endothelial cells, and fibroblasts, was developed to engineer a physiologically relevant cardiac tissue model using a 3D culture system, various biomaterials and bioprinting technology [10, 13, 53, 66–69]. These multicellular spheroids and 3D models will be applied for developing cardiac fibrosis models by introducing external fibrotic signals. Moreover, when developing in vitro cardiac fibrosis models for personalized drug efficacy and toxicity testing, the iPSC technology applied in this study enables the creation of in vitro disease models in which various cell types with the same genetic background can be assembled. Therefore, disease models using patient-specific cells can be used as platforms to explore new therapies by providing individually optimized treatments.

In this work, we established a 3D in vitro model of cardiac fibrosis using 3D cardiac microtissues by treatment with TGF- β 1, which is a potent stimulator that promotes the differentiation and proliferation of myofibroblasts during the course of this disease [70]. Our in vitro model, long-term treatment of TGF- β 1 induces irregular beating patterns (Fig. 5a), an increase in the accumulation of fibrillar collagen deposition (Fig. 5b), elevated expression of α -SMA, conversion to myofibroblasts (Fig. 5f), increase in the rate of apoptosis of CMs (Fig. 5c, d), and disruption of the mitochondrial network as shown by transformation of filamentous into punctate mitochondria (Fig. 6c), consistent with the pathological

changes during cardiac fibrosis [70, 71]. However, we did not detect increased proliferation of MSC or trans-differentiated myofibroblasts in response to TGF- β 1 treatment (data not shown), which may have been due to the inclusion of serum-free medium in the cardiac sphere culture conditions. Moreover, we examined whether 3D cardiac microtissues could be used to detect and monitor cardiac fibrosis using known pro-fibrotic mediators. After a 2-week exposure to pro-fibrotic mediators, including bisphenol A, aldosterone and metoprolol, 3D cardiac microtissues display fibrotic features (Fig. 7a-g), such as an up-regulation of pro-fibrotic and TGF- β 1-responsive genes, collagen secretion and deposition; increased α -SMA expression; and disorganization of the mitochondrial network, leading to mitochondrial fragmentation, without significant differences compared to TGF- β 1-treated cardiac microtissues. These results suggested that our 3D cardiac model can be applied to identify thus far unknown fibrotic compounds and to provide a platform for studying mechanisms of cardiac fibrosis. However, the expression levels of TGF- β 1 responsive genes varied among pro-fibrotic drugs (Fig. 7a), suggesting that there may be different detailed molecular mechanisms for the activation of the TGF- β 1 pathway. The link between pro-fibrotic drugs and the TGF- β 1 pathway is very complex since different molecular mechanisms are involved. Therefore, this research model could provide the basics for studying the development of cardiac fibrosis in response to the different drugs.

However, we recognize the limitations of this in vitro model in recapitulating human diseases, as it lacks adequate blood flow and other physiological factors, such as endothelial and inflammatory cells, which are found in the native heart. There is also a need to apply natural and synthetic biomaterials mimicking native ECMs, as biomaterials play a major role in constructing 3D tissue models via supporting cell attachment and alignment and providing tissue-relevant stiffness [72]. Therefore, the further introduction of various cell types present in the heart, application of microfluidics, and use of tissue engineering strategies can be exploited in the development of physiologically relevant in vitro human heart tissue.

Conclusions

In this study, we report a simplified cardiac microtissue comprising CMs and MSCs derived from hESCs to study cardiac fibrosis in a 3D spheroid platform. Our study highlights the importance of increasing the cellular complexity by adding the appropriate amount of CD44-positive MSCs which can contribute to cardiac fibrosis by generating fibroblasts to better model human cardiac tissues in vitro. Because our cardiac tissue model can be adapted to mimic various aspects of cardiac

fibrosis, it cannot only be used to provide further insights into the mechanisms underlying cardiac fibrosis but can also potentially contribute to the development of in vitro assay systems for testing pro-fibrotic compounds and new anti-fibrotic therapies.

Methods

Cell culture

H9 hESCs were obtained from the WiCell Research Institute (Madison, WI, USA) and maintained as described previously [73]. This study using human embryonic stem cell lines was approved by the Public Institutional Bioethics Committee designated by the Ministry of Health and Welfare (MoHW) (Seoul, Republic of Korea; IRB no. P01-201409-ES-01).

Differentiation of hESCs into human CMs

Human cardiomyocytes were differentiated as described previously [24]. hESCs were transferred to Matrigel (BD Bioscience, San Jose, CA)-coated plates with mTESR medium (Stem Cell Technologies, Vancouver, Canada) without feeder cells; then, cells were grown to 90% confluency. For mesoderm induction, hESCs were treated with 6 μ M CHIR99021 (Tocris, Bristol, UK) for 2 days in Cardiac Differentiation Medium (CDM) consisting of RPMI1640 supplemented with 50 μ g/ml L-ascorbic acids (Sigma-Aldrich, St. Louis, MO, USA) and 500 μ g/ml recombinant albumin (Sigma-Aldrich). Cardiac specification was performed by treating with 2 μ M of Wnt-C59 (Selleck Chemicals, Houston, TX, USA) for another 2 days in CDMs. Subsequently, the cells were replaced with CDM medium once every two days until beating CMs were observed. Differentiated CMs were maintained in RPMI-B27 medium consisting of RPMI1640 supplemented with 50 μ g/ml L-ascorbic acids and 1XB27 (Thermo Fisher Scientific, Waltham, MA, USA).

Differentiation of hESC into human MSCs

Human MSCs were differentiated from hESCs as described previously [74]. hESCs were transferred to Matrigel-coated plates with mTESR medium (Stem Cell Technologies) without feeder cells; then, cells were grown to 50% confluency. For mesenchymal differentiation, medium was changed to MEM- α supplemented with 10% FBS and 5 ng/ml bFGF (R&D Systems, Minneapolis, MN, USA) once every two days. Cells were transferred to a gelatine-coated dish every week.

Generation of CM-MSC cardiac microtissues

The differentiated CM and MSC cells were dissociated into single cells by 0.25% trypsin treatment, and the number of cells was counted with a haemocytometer. The CMs and MSCs were mixed at a ratio of 4:1, and 50,000 cells per well were seeded in a 96 well ultra-low

attachment plate with RPMI-B27 media supplemented with 10% FBS. After the sphere formation was completed within 2–3 days, the medium was replaced with RPMI-B27 and the medium was replaced every 2–3 days. To develop the *in vitro* fibrosis model, 5 ng/ml TGF- β 1 or 10 μ M concentration of each cardiotoxic chemical, including Bisphenol A, Aldosterone, and Metoprolol (all reagents from Sigma-Aldrich) were treated independently with the indicated concentration of drugs as described in previous reports [36–38] and the samples were harvested for analysis after 2 weeks.

FACS analysis

To verify the CM and MSC differentiation efficiency, FACS analysis was performed as described previously [75]. The differentiated CMs and MSCs were treated with 0.25% trypsin, dissociated into single cells, and incubated in dPBS containing 2 mM EDTA and 2% FBS for 10 min. After that, antibodies to the surface markers of each cell (Additional file 9: Table S1) were diluted 1:50 and reacted for 30 min. After washing twice with FACS buffer, FACS analysis was performed using Accuri C6 flow cytometry (BD Biosciences) and analysed using FlowJo V10 software (TreeStar, USA).

Processing of cardiac microtissue, immunostaining and MT staining

Cardiac microtissues were fixed by 4% paraformaldehyde (PFA), cryo-protected in 10%~30% sucrose solution and frizzed after embedding in optimal-cutting-temperature (OCT) compound (Sakura Finetek, Tokyo, Japan) as described previously [76]. Frozen section were prepared by cutting at a thickness of 10–15 μ m using a cryostat microtome. The frozen sections were permeabilized with 0.1% Triton X-100 for immune-staining, blocked with 3% BSA, and incubated with the primary antibody (Additional file 9: Table S1). For immunofluorescence detection, cells were incubated with a fluorescence-conjugated secondary antibody. For immunoperoxidase detection, the sections were incubated with the biotinylated secondary antibody and then followed using the VECTASTAIN elite ABC kit (Cat. NO. PK-6100, vector laboratories) and DAB substrate kit (Cat. NO. SK-4100, Vector Laboratories, Burlingame, CA, USA). Staining of collagen fibres was performed using Masson's Trichrome staining kit (Cat no. 25088–1, Polysciences, Inc. Warrington, USA).

Quantitative RT-PCR (qPCR)

To compare mRNA expression levels, total RNA was extracted according to the manufacturer's protocol using the easyBLUE RNA extraction kit (iNtRON Biotechnology, Inc., Republic of Korea). cDNA was synthesized using the SuperScript™ IV First-strand Synthesis System (Cat.NO.1891050, Thermo Fisher Scientific), and the cDNA was used as a

template for real-time qPCR. PCR reactions were performed three times independently using Fast SYBR™ Green Master Mix (4,385,612, Applied Biosystems, Foster City, CA, USA). The sequence of the gene-specific primers are presented in the Additional file 10: Table S2.

Transcriptome analysis by microarray

For global transcriptome analysis, cDNA microarray was performed using an Agilent Human GE (V2) 4 X 44 K chip as described previously [77]. Data were normalized by using GeneSpring software, and differentially expressed genes (DEGs) were analysed by MultiExperiment Viewer software (MeV version 4.9.0; <http://mev.tm4.org/>). Pathway enrichment analysis was performed by Reactome FI plugin of the Cytoscape software (Version 3.2.0, www.cytoscape.org), and gene set enrichment analysis was performed by GSEA 2.2.4 (<http://software.broadinstitute.org/gsea/index.jsp>). The H (hallmark genesets) subsets of MSigDB (50 gene sets), C5_BP (GO biological process, 4436 gene sets) and C5_CC (GO cellular component, 580 gene sets) were used in this study [78].

Beating rate analysis of CM-MSC microtissue by tracing of microscopic video files

Beating rates of CM-MSC microtissue were recorded on a microscope (IX83, Olympus, Japan) with an on-stage incubator (Live Cell Instrument, Seoul, South Korea) at 37 °C and 5% CO₂ to maintain the physiological condition. The plot z-axis profile of each region of interest (ROI) was calculated by Image J software (<https://imagej.nih.gov/ij/>) program [79].

Field potential recordings using a multi-electrode array (MEA) system

The hESC-derived CMs were plated on a Matrigel-coated 12-well MEA plate (4×10^4 cell per well) (AXION, Atlanta, GA, USA) in RPMI-B27 media supplemented with 5% FBS. At 24 h after seeding, the medium was replaced with RPMI-B27. Field potentials were recorded at day 6 after seeding using Axion BioSystems' Maestro MEA systems set as 37 °C and perfused with 5% CO₂, 20% O₂, and 75% N₂. Field potential signals were recorded with Axion BioSystems' Integrated Studio (AxIS) software version 2.3 and analysed with the Axion Cardiac Data Plotting Tool.

Statistical analysis and graph drawing

Whether treatments produce significantly different results was evaluated by statistical analysis. The unpaired t-test (Figs. 1c, 2c, 3b, e, 4e, 5d, and e) and one-way ANOVA followed by Dunnett's multiple comparisons test (Fig. 7a, d, and e) were performed using GraphPad Prism version 6.00 for Windows (GraphPad Software, Inc., USA).

Additional files

Additional file 1: Movie 1. Cardiomyocytes derived from hESCs. (MP4 9007 kb)

Additional file 2: Figure S1. Effect of TGF- β 1 in CM spheroid. (A) Representative morphology of hESC-derived CM spheroids with or without TGF- β 1 treatment for 3 weeks. (B) Masson's Trichrome staining to visualize collagen fibers in CM spheroids. Scale bars, 100 μ m. (MP4 4521 kb)

Additional file 3: Movie 2. Cardiac spheroid of hESC-derived CMs on day 14. (MP4 4700 kb)

Additional file 4: Movie 3. Cardiac spheroid comprising both hESC-derived CMs and MSCs on day 14. (MP4 1623 kb)

Additional file 5: Movie 4. TGF- β 1-treated cardiac spheroid comprising both hESC-derived CMs and MSCs on day 14. (MP4 1768 kb)

Additional file 6: Figure S2. Collagen deposition in TGF- β 1 treated CM-MSC microtissue. Masson's Trichrome staining to visualize collagen fibres in multiple sections of CM spheroids at 14 days after 5 ng/ml TGF- β 1 treatment. Scale bars, 100 μ m. (TIF 5720 kb)

Additional file 7: Figure S3. Comparative cellular component analysis of control and TGF- β 1-induced fibrosis models. Gene set enrichment analysis (GSEA) of transcriptome data in TGF- β 1 induced fibrosis model was performed by MSigDB of GO cellular component (580 gene set). (A) List of gene sets enriched in cardiac fibrosis model was shown by normalized enrichment score (NES) and false discovery rate (FDR). Enrichment plot of top ranked subset; proteinaceous extracellular matrix and basement membrane. (B) List of gene sets enriched in control was shown by NES and FDR value. Enrichment plot of top ranked subset, respiratory chain and inner mitochondrial membrane protein complex. (TIF 2203 kb)

Additional file 8: Figure S4. Treatment of hESC-derived CMs with profibrotic drugs. (A) Immunofluorescent staining of apoptotic CMs with an apoptosis-specific marker (Cleaved caspase 3; Cl-Casp3). Scale bars, 50 μ m. Percentage of apoptotic CMs by quantifying ratio of Cl-Casp3 positive cells per number of DAPI-stained cells. (C) Immunofluorescence staining of mitochondrial-specific marker (TOM20). Nuclei were stained with DAPI (blue). Scale bars, 10 μ m. (TIF 5406 kb)

Additional file 9: Table S1. List of the antibodies used in this study. (DOCX 16 kb)

Additional file 10: Table S2. List of the primers used in this study. (DOCX 16 kb)

Abbreviation

2D: Two dimensional; 3D: Three dimensional; CDM: Cardiac differentiation medium; CM: Cardiomyocyte; cTnT: Cardiac muscle troponin T; Cx43: Connexin 43; DEG: Differentially expressed gene; ECM: Extracellular matrix; EMT: Epithelial-mesenchymal transition; Endo-MT: Endothelial-mesenchymal transition; FA: Fatty acid; FP: Field potential; FPD: Field potential duration; GSEA: Gene set enrichment analysis; hESC: Human embryonic stem cell; hiPSC: Human induced pluripotent stem cell; hPSC: Human pluripotent stem cell; MSC: Mesenchymal stem cell; OCT: Optimal-cutting-temperature; PC1: Principal component 1; PC2: Principal component 2; PFA: Paraformaldehyde; SAA: Sarcomeric alpha-actinin; TGF- β 1: Transforming growth factor β 1; α -SMA: α -smooth muscle actin

Acknowledgements

Not applicable.

Funding

This work was supported by a grant from the Technology Innovation Program (No. 10063334) funded by the Ministry of Trade, Industry & Energy (M, Korea), the National Research Foundation of Korea (NRF) grant funded by the Ministry of Science, ICT and Future Planning (2018R1C1B6008256 and NRF-2018M3A9H3023077), and the KRIBB Research Initiative Program. The funders had no role in the study design, data collection or analysis, decision to publish, or preparation of the manuscript.

Availability of data and materials

All data generated or analyzed during this study are included in this published article and its additional files.

Authors' contributions

MOL designed the studies, performed the experiments, analysed the data and prepared the manuscript. KBJ and JSJ performed the experiments and analysed the data. SAH, KSM, and JWS performed and analysed the MEA experiments. SHK and MYS planned the project, analysed the data, wrote and critically revised the manuscript. All authors read and approved the final manuscript.

Ethics approval and consent to participate

Not applicable.

Consent for publication

Not applicable.

Competing interests

The authors declare that they have no competing interests.

Publisher's Note

Springer Nature remains neutral with regard to jurisdictional claims in published maps and institutional affiliations.

Author details

¹Stem Cell Convergence Research Center, Korea Research Institute of Bioscience and Biotechnology (KRIBB), Daejeon 341411, Republic of Korea. ²Department of Functional Genomics, KRIBB School of Bioscience, Korea University of Science and Technology (UST), Daejeon 34113, Republic of Korea. ³Research Group for Safety Pharmacology, Korea Institute of Toxicology, KRICT, Daejeon 34114, Republic of Korea. ⁴Center for Biomaterials, Korea Institute of Science and Technology (KIST), Seoul 02792, Republic of Korea. ⁵Department of Biomedical Engineering, KIST school, UST, Daejeon 34113, Republic of Korea.

Received: 19 September 2018 Accepted: 2 January 2019

Published online: 13 February 2019

References

- Sutra T, Oiry C, Azay-Milhau J, Youl E, Magous R, Teissedre PL, Cristol JP, Cros G. Preventive effects of nutritional doses of polyphenolic molecules on cardiac fibrosis associated with metabolic syndrome: involvement of osteopontin and oxidative stress. *J Agric Food Chem*. 2008;56(24):11683–7.
- Tian J, An X, Niu L. Myocardial fibrosis in congenital and pediatric heart disease. *Exp Ther Med*. 2017;13(5):1660–4.
- Travers JG, Kamal FA, Robbins J, Yutzey KE, Blaxall BC. Cardiac fibrosis: the fibroblast awakens. *Circ Res*. 2016;118(6):1021–40.
- Murtha LA, Schuliga MJ, Mabotuwana NS, Hardy SA, Waters DW, Burgess JK, Knight DA, Boyle AJ. The processes and mechanisms of cardiac and pulmonary fibrosis. *Front Physiol*. 2017;8:777.
- Ottaviano FG, Yee KO. Communication signals between cardiac fibroblasts and cardiac myocytes. *J Cardiovasc Pharmacol*. 2011;57(5):513–21.
- Rockey DC, Bell PD, Hill JA. Fibrosis—A Common pathway to organ injury and failure. *N Engl J Med*. 2015;373(1):96.
- Weber KT, Sun Y, Bhattacharya SK, Ahokas RA, Gerling IC. Myofibroblast-mediated mechanisms of pathological remodelling of the heart. *Nat Rev Cardiol*. 2013;10(1):15–26.
- Figtree GA, Bubbs KJ, Tang O, Kizana E, Gentile C. Vascularized cardiac spheroids as novel 3D in vitro models to study cardiac fibrosis. *Cells Tissues Organs*. 2017;204(3–4):191–8.
- Galie PA, Stegemann JP. Injection of mesenchymal stromal cells into a mechanically stimulated in vitro model of cardiac fibrosis has paracrine effects on resident fibroblasts. *Cytotherapy*. 2014;16(7):906–14.
- Sadeghi AH, Shin SR, Deddens JC, Fratta G, Mandla S, Yazdi IK, Prakash G, Antona S, Demarchi D, Buijsrogge MP, et al. Engineered 3D cardiac fibrotic tissue to study fibrotic remodeling. *Adv Healthc Mater*. 2017;6(11):1601434.
- Zhao H, Li X, Zhao S, Zeng Y, Zhao L, Ding H, Sun W, Du Y. Microengineered in vitro model of cardiac fibrosis through modulating myofibroblast mechanotransduction. *Biofabrication*. 2014;6(4):045009.

12. van Spreeuwel ACC, Bax NAM, van Nierop BJ, Aartsma-Rus A, Goumans MTH, Bouten CVC. Mimicking cardiac fibrosis in a dish: fibroblast density rather than collagen density weakens cardiomyocyte function. *J Cardiovasc Transl Res*. 2017;10(2):116–27.
13. Polonchuk L, Chabria M, Badi L, Hoflack JC, Figtree G, Davies MJ, Gentile C. Cardiac spheroids as promising in vitro models to study the human heart microenvironment. *Sci Rep*. 2017;7(1):7005.
14. Yamashita JK. ES and iPSC cell research for cardiovascular regeneration. *Exp Cell Res*. 2010;316(16):2555–9.
15. van den Berg CW, Elliott DA, Braam SR, Mummery CL, Davis RP. Differentiation of human pluripotent stem cells to cardiomyocytes under defined conditions. *Methods Mol Biol*. 2016;1353:163–80.
16. Birket MJ, Mummery CL. Pluripotent stem cell derived cardiovascular progenitors—a developmental perspective. *Dev Biol*. 2015;400(2):169–79.
17. Jugdutt BI. Ventricular remodeling after infarction and the extracellular collagen matrix: when is enough enough? *Circulation*. 2003;108(11):1395–403.
18. Carlson S, Trial J, Soeller C, Entman ML. Cardiac mesenchymal stem cells contribute to scar formation after myocardial infarction. *Cardiovasc Res*. 2011;91(1):99–107.
19. Mollmann H, Nef HM, Kostin S, von Kalle C, Pilz I, Weber M, Schaper J, Hamm CW, Elsasser A. Bone marrow-derived cells contribute to infarct remodelling. *Cardiovasc Res*. 2006;71(4):661–71.
20. van Amerongen MJ, Bou-Gharios G, Popa E, van Ark J, Petersen AH, van Dam GM, van Luyn MJ, Harnsen MC. Bone marrow-derived myofibroblasts contribute functionally to scar formation after myocardial infarction. *J Pathol*. 2008;214(3):377–86.
21. Cieslik KA, Trial J, Entman ML. Defective myofibroblast formation from mesenchymal stem cells in the aging murine heart rescue by activation of the AMPK pathway. *Am J Pathol*. 2011;179(4):1792–806.
22. Kanisicak O, Khalil H, Ivey MJ, Karch J, Maliken BD, Correll RN, Brody MJ, SC JL, Aronow BJ, Tallquist MD, et al. Genetic lineage tracing defines myofibroblast origin and function in the injured heart. *Nat Commun*. 2016;7:12260.
23. El Agha E, Kramann R, Schneider RK, Li X, Seeger W, Humphreys BD, Bellusci S. Mesenchymal stem cells in fibrotic disease. *Cell Stem Cell*. 2017;21(2):166–77.
24. Burrige PW, Matsa E, Shukla P, Lin ZC, Churko JM, Ebert AD, Lan F, Diecke S, Huber B, Mordwinkin NM, et al. Chemically defined generation of human cardiomyocytes. *Nat Methods*. 2014;11(8):855–60.
25. Fromaget C, el Aoumari A, Gros D. Distribution pattern of connexin 43, a gap junctional protein, during the differentiation of mouse heart myocytes. *Differentiation*. 1992;51(1):9–20.
26. Delmar M, Liang FX. Connexin43 and the regulation of intercalated disc function. *Heart Rhythm*. 2012;9(5):835–8.
27. Dobaczewski M, Chen W, Frangogiannis NG. Transforming growth factor (TGF)-beta signaling in cardiac remodeling. *J Mol Cell Cardiol*. 2011;51(4):600–6.
28. Chen QM, Maltagliati AJ. Nrf2 at the heart of oxidative stress and cardiac protection. *Physiol Genomics*. 2018;50(2):77–97.
29. Li J, Dai Y, Su Z, Wei G. MicroRNA-9 inhibits high glucose-induced proliferation, differentiation and collagen accumulation of cardiac fibroblasts by down-regulation of TGFBR2. *Biosci Rep*. 2016;36(6):e00417.
30. Zhou P, Pu WT. Recounting cardiac cellular composition. *Circ Res*. 2016;118(3):368–70.
31. Johnstone AF, Gross GW, Weiss DG, Schroeder OH, Gramowski A, Shafer TJ. Microelectrode arrays: a physiologically based neurotoxicity testing platform for the 21st century. *Neurotoxicology*. 2010;31(4):331–50.
32. Goldsmith EC, Hoffman A, Morales MO, Potts JD, Price RL, McFadden A, Rice M, Borg TK. Organization of fibroblasts in the heart. *Dev Dyn*. 2004;230(4):787–94.
33. Ilkun O, Boudina S. Cardiac dysfunction and oxidative stress in the metabolic syndrome: an update on antioxidant therapies. *Curr Pharm Des*. 2013;19(27):4806–17.
34. Mali VR, Pan G, Deshpande M, Thandavarayan RA, Xu J, Yang XP, Palaniyandi SS. Cardiac mitochondrial respiratory dysfunction and tissue damage in chronic hyperglycemia correlate with reduced aldehyde Dehydrogenase-2 activity. *PLoS One*. 2016;11(10):e0163158.
35. Nagoshi T, Yoshimura M, Rosano GM, Lopaschuk GD, Mochizuki S. Optimization of cardiac metabolism in heart failure. *Curr Pharm Des*. 2011;17(35):3846–53.
36. Hu Y, Zhang L, Wu X, Hou L, Li Z, Ju J, Li Q, Qin W, Li J, Zhang Q, et al. Bisphenol a, an environmental estrogen-like toxic chemical, induces cardiac fibrosis by activating the ERK1/2 pathway. *Toxicol Lett*. 2016;250-251:1–9.
37. Brilla CG. Aldosterone and myocardial fibrosis in heart failure. *Herz*. 2000;25(3):299–306.
38. Nakaya M, Chikura S, Watari K, Mizuno N, Mochinaga K, Mangmool S, Koyanagi S, Ohdo S, Sato Y, Ide T, et al. Induction of cardiac fibrosis by beta-blocker in G protein-independent and G protein-coupled receptor kinase 5/beta-arrestin2-dependent signaling pathways. *J Biol Chem*. 2012;287(42):35669–77.
39. Baum J, Duffy HS. Fibroblasts and myofibroblasts: what are we talking about? *J Cardiovasc Pharmacol*. 2011;57(4):376–9.
40. Eder A, Vollert I, Hansen A, Eschenhagen T. Human engineered heart tissue as a model system for drug testing. *Adv Drug Deliv Rev*. 2016;96:214–24.
41. Nunes SS, Miklas JW, Liu J, Aschar-Sobbi R, Xiao Y, Zhang B, Jiang J, Masse S, Gagliardi M, Hsieh A, et al. Biowire: a platform for maturation of human pluripotent stem cell-derived cardiomyocytes. *Nat Methods*. 2013;10(8):781–7.
42. Zuppinger C. 3D culture for cardiac cells. *Biochim Biophys Acta*. 2016;1863(7 Pt B):1873–81.
43. Wakili R, Voigt N, Kaab S, Dobrev D, Nattel S. Recent advances in the molecular pathophysiology of atrial fibrillation. *J Clin Invest*. 2011;121(8):2955–68.
44. Porter KE, Turner NA. Cardiac fibroblasts: at the heart of myocardial remodeling. *Pharmacol Ther*. 2009;123(2):255–78.
45. Souders CA, Bowers SL, Baudino TA. Cardiac fibroblast: the renaissance cell. *Circ Res*. 2009;105(12):1164–76.
46. Camelliti P, Borg TK, Kohl P. Structural and functional characterisation of cardiac fibroblasts. *Cardiovasc Res*. 2005;65(1):40–51.
47. Doppler SA, Carvalho C, Lahm H, Deutsch MA, Dressen M, Puluca N, Lange R, Krane M. Cardiac fibroblasts: more than mechanical support. *J Thorac Dis*. 2017;9(Suppl 1):S36–51.
48. Pellman J, Zhang J, Sheikh F. Myocyte-fibroblast communication in cardiac fibrosis and arrhythmias: mechanisms and model systems. *J Mol Cell Cardiol*. 2016;94:22–31.
49. Son MY, Lee MO, Jeon H, Seol B, Kim JH, Chang JS, Cho YS. Generation and characterization of integration-free induced pluripotent stem cells from patients with autoimmune disease. *Exp Mol Med*. 2016;48:e232.
50. Olivier EN, Rybicki AC, Bouhassira EE. Differentiation of human embryonic stem cells into bipotent mesenchymal stem cells. *Stem Cells*. 2006;24(8):1914–22.
51. Lee CH, Shah B, Moiola EK, Mao JJ. CTGF directs fibroblast differentiation from human mesenchymal stem/stromal cells and defines connective tissue healing in a rodent injury model. *J Clin Invest*. 2010;120(9):3340–9.
52. Nesselmann C, Ma N, Bieback K, Wagner W, Ho A, Kontinen YT, Zhang H, Hinescu ME, Steinhoff G. Mesenchymal stem cells and cardiac repair. *J Cell Mol Med*. 2008;12(5B):1795–810.
53. Ong CS, Fukunishi T, Zhang H, Huang CY, Nashed A, Blazeski A, DiSilvestre D, Vricella L, Conte J, Tung L, et al. Biomaterial-free three-dimensional bioprinting of cardiac tissue using human induced pluripotent stem cell derived cardiomyocytes. *Sci Rep*. 2017;7(1):4566.
54. Cui X, Hartanto Y, Zhang H. Advances in multicellular spheroids formation. *J R Soc Interface*. 2017;14(127):20160877.
55. DeLeon-Pennell KY. May the fibrosis be with you: is discoidin domain receptor 2 the receptor we have been looking for? *J Mol Cell Cardiol*. 2016;91:201–3.
56. Ivey MJ, Tallquist MD. Defining the cardiac fibroblast. *Circ J*. 2016;80(11):2269–76.
57. Gabbiani G. The cellular derivation and the life span of the myofibroblast. *Pathol Res Pract*. 1996;192(7):708–11.
58. Jeon ES, Moon HJ, Lee MJ, Song HY, Kim YM, Cho M, Suh DS, Yoon MS, Chang CL, Jung JS, et al. Cancer-derived lysophosphatidic acid stimulates differentiation of human mesenchymal stem cells to myofibroblast-like cells. *Stem Cells*. 2008;26(3):789–97.
59. Kuppe C, Kramann R. Role of mesenchymal stem cells in kidney injury and fibrosis. *Curr Opin Nephrol Hypertens*. 2016;25(4):372–7.
60. Ozen I, Boix J, Paul G. Perivascular mesenchymal stem cells in the adult human brain: a future target for neuroregeneration? *Clin Transl Med*. 2012;1(1):30.
61. Ngo MA, Muller A, Li Y, Neumann S, Tian G, Dixon IM, Arora RC, Freed DH. Human mesenchymal stem cells express a myofibroblastic phenotype in

- vitro: comparison to human cardiac myofibroblasts. *Mol Cell Biochem.* 2014; 392(1–2):187–204.
62. Waxse BJ, Sengupta P, Hesketh GG, Lippincott-Schwartz J, Buss F. Myosin VI facilitates connexin 43 gap junction accretion. *J Cell Sci.* 2017;130(5):827–40.
 63. Davis RP, van den Berg CW, Casini S, Braam SR, Mummery CL. Pluripotent stem cell models of cardiac disease and their implication for drug discovery and development. *Trends Mol Med.* 2011;17(9):475–84.
 64. Zeevi-Levin N, Itskovitz-Eldor J, Binah O. Cardiomyocytes derived from human pluripotent stem cells for drug screening. *Pharmacol Ther.* 2012; 134(2):180–8.
 65. Moretti A, Laugwitz KL, Dorn T, Sinnecker D, Mummery C. Pluripotent stem cell models of human heart disease. *Cold Spring Harb Perspect Med.* 2013; 3(11):a014027.
 66. Archer CR, Sargeant R, Basak J, Pilling J, Barnes JR, Pointon A. Characterization and validation of a human 3D cardiac microtissue for the assessment of changes in cardiac pathology. *Sci Rep.* 2018;8(1):10160.
 67. Emmert MY, Wolint P, Wickboldt N, Gemayel G, Weber B, Brokopp CE, Boni A, Falk V, Bosman A, Jaconi ME, et al. Human stem cell-based three-dimensional microtissues for advanced cardiac cell therapies. *Biomaterials.* 2013;34(27):6339–54.
 68. Wang L, Huang G, Sha B, Wang S, Han YL, Wu J, Li Y, Du Y, Lu TJ, Xu F. Engineering three-dimensional cardiac microtissues for potential drug screening applications. *Curr Med Chem.* 2014;21(22):2497–509.
 69. Giacomelli E, Bellin M, Sala L, van Meer BJ, Tertoolen LG, Orlova VV, Mummery CL. Three-dimensional cardiac microtissues composed of cardiomyocytes and endothelial cells co-differentiated from human pluripotent stem cells. *Development.* 2017;144(6):1008–17.
 70. Bujak M, Frangogiannis NG. The role of TGF- β signaling in myocardial infarction and cardiac remodeling. *Cardiovasc Res.* 2007;74(2):184–95.
 71. Wei B, Cai L, Sun D, Wang Y, Wang C, Chai X, Xie F, Su M, Ding F, Liu J, et al. Microsomal prostaglandin E synthase-1 deficiency exacerbates pulmonary fibrosis induced by bleomycin in mice. *Molecules.* 2014;19(4):4967–85.
 72. Mathur A, Ma Z, Loskill P, Jeeawoody S, Healy KE. In vitro cardiac tissue models: current status and future prospects. *Adv Drug Deliv Rev.* 2016;96:203–13.
 73. Jung KB, Son YS, Lee H, Jung CR, Kim J, Son MY. Transcriptome dynamics of human pluripotent stem cell-derived contracting cardiomyocytes using an embryoid body model with fetal bovine serum. *Mol BioSyst.* 2017;13(8):1565–74.
 74. Lee MO, You CH, Son MY, Kim YD, Jeon H, Chang JS, Cho YS. Pro-fibrotic effects of PFKFB4-mediated glycolytic reprogramming in fibrous dysplasia. *Biomaterials.* 2016;107:61–73.
 75. Jung KB, Lee H, Son YS, Lee MO, Kim YD, Oh SJ, Kwon O, Cho S, Cho HS, Kim DS, et al. Interleukin-2 induces the in vitro maturation of human pluripotent stem cell-derived intestinal organoids. *Nat Commun.* 2018;9(1):3039.
 76. Jung KB, Lee H, Son YS, Lee JH, Cho HS, Lee MO, Oh JH, Lee J, Kim S, Jung CR, et al. In vitro and in vivo imaging and tracking of intestinal organoids from human induced pluripotent stem cells. *FASEB J.* 2018;32(1):111–22.
 77. Son MY, Sim H, Son YS, Jung KB, Lee MO, Oh JH, Chung SK, Jung CR, Kim J. Distinctive genomic signature of neural and intestinal organoids from familial Parkinson's disease patient-derived induced pluripotent stem cells. *Neuropathol Appl Neurobiol.* 2017;43(7):584–603.
 78. Liberzon A, Birger C, Thorvaldsdottir H, Ghandi M, Mesirov JP, Tamayo P. The molecular signatures database (MSigDB) hallmark gene set collection. *Cell Syst.* 2015;1(6):417–25.
 79. Jaffer S, Valasek P, Luke G, Batarfi M, Whalley BJ, Patel K. Characterisation of development and electrophysiological mechanisms underlying rhythmicity of the avian lymph heart. *PLoS One.* 2016;11(12):e0166428.

Ready to submit your research? Choose BMC and benefit from:

- fast, convenient online submission
- thorough peer review by experienced researchers in your field
- rapid publication on acceptance
- support for research data, including large and complex data types
- gold Open Access which fosters wider collaboration and increased citations
- maximum visibility for your research: over 100M website views per year

At BMC, research is always in progress.

Learn more [biomedcentral.com/submissions](https://www.biomedcentral.com/submissions)

